Spatial Patterns of Glacial Erosion at a Valley Scale Derived From Terrestrial Cosmogenic ^{10}Be and ^{26}Al Concentrations in Rock

Derek Fabel,[1],* Jon Harbor,[1] Dennis Dahms,[2] Allan James,[3] David Elmore,[4] Linda Horn,[1] Kelly Daley,[1] and Charles Steele[1]

[1]Department of Earth and Atmospheric Sciences, Purdue University
[2]Department of Geography, University of Northern Iowa
[3]Department of Geography, University of South Carolina
[4]Department of Physics, Purdue University
*now at: Research School of Earth Sciences, Australian National University, Australia

The fundamentally geographic issue of the amounts and spatial patterns of erosion necessary to produce classic glacial landforms such as U-shaped valleys has been debated by scientists for over a century. Terrestrial cosmogenic nuclide (TCN) measurements in glacially abraded bedrock were used to determine patterns of glacial erosion and to quantify the amount of rock removed during the last glaciation along valley-side transects in Sinks Canyon, Wind River Range, Wyoming, and the South Yuba River, Sierra Nevada, California. Surface exposure ages from bedrock and erratic samples obtained during this study indicate last deglaciation between 13–18 ka in the South Yuba River and 15–17 ka in Sinks Canyon. These ages are in agreement with previously published glacial chronologies. In both areas, samples from valley cross sections revealed a pattern of erosion during the last glaciation that decreased toward the lateral limit of ice extent, as predicted by numerical models, while transects further upstream recorded >1.4 meters of bedrock removal throughout. The effects of varying interglacial erosion and surface exposure histories on modeled glacial erosion depths were tested, validating the methodology used. The results demonstrate that the TCN technique, applied at the valley scale, provides useful insight into the spatial pattern of glacial erosion. Extensive sampling in areas with limited erosional loss may provide detailed records of erosion patterns with which to test predictions generated by models of ice dynamics and erosion processes. *Key Words: cosmogenic nuclides, glacial erosion, Sierra Nevada, Wind River Range.*

Natural landforms result from spatial and temporal variations in the effectiveness of weathering and erosion and from rock formation and tectonic processes. Given the long history of environmental and geologic change that has affected many landscapes, understanding how the present topographic form of an area developed typically requires consideration of a wide range of processes operating over diverse time and space scales (e.g., Thorn 1982). Although complex palimpsest landscapes are common (e.g., Kleman 1992; Parent, Paradis, and Doiron 1996; Kehew, Nicks, and Straw 1999), in many areas the landscape reflects the dominant overprint of a small set of controls or processes. The recognition of such dominant patterns has led geomorphologists to organize landscapes and landforms into groups that reflect the outcome of common governing processes or environmental controls. For example, we recognize distinct landform assemblages related to dominant glacial or fluvial processes (e.g., Sugden and John 1976; Schumm 1977) and typically describe unique groupings of landforms and landscapes associated with particular climatic or tectonic settings (e.g., Morisawa 1976; Bull 1991). Modern geomorphology includes a focus on understanding the governing processes and controls that underlie these classifications and the use of this knowledge both for environmental management and as the foundation for understanding the development of specific landforms and landscape types (e.g., Chorley, Schumm, and Sugden 1984; Selby 1986).

To develop and test process-based explanations of landform and landscape evolution under a dominant process regime is challenging. This is particularly true when the timescale of form development exceeds that over which direct observations of processes and form change can be made and where the spatial scale of process measurements is different from that of form change. For example, it would be hard to understand the formation of the Grand Canyon simply by observing the processes in a small section of the system over a few years. A typical strategy to address this challenge involves initial development of process models from first

principles and small-time and space-scale observations, followed by the use of these models to predict form development over much larger space and time scales to test against observed changes in form (e.g., Howard, Dietrich, and Seidl 1994; Tucker and Slingerland 1994; Braun, Zwartz, and Tomkin 1999).

Determinations of past change in form against which we may compare model predictions is particularly challenging for erosional processes at large scales, such as valley-scale patterns of glacial erosion. Such comparisons usually involve either time-space substitution or comparison of present and reconstructed forms. In time-space substitution (use of the ergodic hypothesis, e.g., Oberlander 1985), observations of topographic form at different points in space that are believed to represent different ages or stages in form development are used as a model for change that would occur over time at one point in space (e.g., Merritts 1996). An alternate approach is to attempt to reconstruct past form at a location by extrapolating topographic profiles from unmodified areas across the study site (Matthes 1930). Limitations to both approaches motivate the search for new methods in which form change in an erosional setting can be reconstructed by combining the current topography with some indirect measure of the amount of material lost at various locations (Brown 1991; Fabel and Finlayson 1992).

Valley-scale glacial landform development is a particularly interesting application with which to test a new approach because, for over a century, scientists have been debating the fundamentally geographic issue of the spatial patterns of erosion necessary to produce classic glacial landforms such as U-shaped valleys (e.g., McGee 1894; Matthes 1930; Boulton 1974; Harbor 1995). This debate includes extensive discussion of the mechanics of processes that might give rise to such erosion patterns (e.g., Johnson 1970; Boulton 1974). However, a fundamental constraint is the lack of a reliable way to observe the actual pattern of bedrock loss. Although we can map present-day topography, the preglacial form is largely unknown. Thus, attempts to derive erosion patterns from landscape change have been based on preglacial topography derived either from an untested assumption of a preglacial V-shaped profile or from extrapolated forms or surfaces outside the glacial limit (Matthes 1930). In terms of testing the process models, the former approach is weak because there is rarely evidence to support the assumption, while the latter approach is limited by uncertainty concerning the correct form of extrapolation and the possibility that entire valley evolution is a result of a complex history of processes and events.

Ideal data for testing glacial erosion models would consist of measures of erosional loss patterns at a valley scale due solely to a single, well-constrained glacial event. New data on actual spatial patterns of erosion resulting from glacial action in an alpine valley would be invaluable in efforts to: (1) clarify and quantify models of glacier mechanics, (2) develop a better understanding of the erosional feedback mechanisms functioning between ice and the surrounding bedrock, and (3) understand how glacier erosion modifies the surrounding bedrock to produce the classic landscapes of mountain geography. In this context it has become clear that TCNs in rock can provide information about past amounts of surface erosion (Elmore et al. 1995; Briner and Swanson 1998; Bierman et al. 1999; Cockburn, Seidl, and Summerfield 1999; Davis et al. 1999; Colgan et al. 2002; Fabel et al. 2002; Stroeven et al. 2002). Quantitative erosion estimates, coupled with approaches that predict spatial patterns of erosion as a function of erosion mechanisms and controls (e.g., Harbor 1992, 1995), have the potential to significantly enhance our understanding of valley-scale erosion patterns and processes.

Terrestrial Cosmogenic Nuclides as Glacial Erosion Monitors

TCNs are produced in rocks near the ground surface by nuclear reactions between minerals and secondary cosmic rays (Lal and Peters 1967). With prolonged exposure, TCNs accumulate within exposed minerals as a function of time and depth below the surface. Time elapsed since initial rock surface exposure, or the steady-state erosion rate of the surface, can be modeled using the accumulated TCN concentrations (Lal 1991; Nishiizumi et al. 1993; Cerling and Craig 1994). Here we use ^{10}Be (half-life $= 1.51 \pm 0.03 \times 10^6$ a; Hofmann et al. 1987) and ^{26}Al (half-life $= 7.05 \pm 0.2 \times 10^5$ a; Norris et al. 1983) concentrations in quartz to derive depth of bedrock removal by glacial erosion at multiple sites across glacial valleys during the last glaciation in these valleys. The concentration of ^{10}Be or ^{26}Al resulting from spallation reactions in quartz exposed at sea level and high latitude ($>60°$) by cosmic ray nucleons (neutrons and some protons) can be expressed as

$$N = N_{inh}e^{-\lambda t} + [P_n e^{-\rho z/\Lambda}/(\lambda + \rho\varepsilon/\Lambda)] \times [1 - e^{-(\lambda + \rho\varepsilon/\Lambda)t}] \tag{1}$$

where N is the TCN concentration, N_{inh} is any nuclide concentration inherited from an earlier exposure period, P_n is the production rate due to neutrons, λ is radioactive decay, ρ is the density of the rock (2.75 g cm^{-3} in this

study), z is the depth below the surface, ε is the surface erosion rate, Λ is the cosmic ray mean free path (160 ± 10 g cm^{-2}), and t is the exposure time. Equation 1 does not take into account nuclear reactions with muons that penetrate much further into rock and become the dominant production pathway at sufficient depth (Figure 1). A simple exponential law can model production by nucleons as a function of depth, but muon production as a function of depth is not readily modeled by a simple analytical expression. Granger and Smith (2000) have shown that, for many purposes, production by muons as a function of depth can be modeled using the sum of three exponential terms, leading to the more complete equation:

$$
\begin{aligned}
N =& N_{inh}\, e^{-\lambda t} + [P_n e^{-\rho z/\Lambda}/(\lambda + \rho\varepsilon/\Lambda)][1 - e^{-(\lambda+\rho\varepsilon/\Lambda)t}] \\
&+ [A_1\, e^{-\rho z/L_1}/(\lambda + \rho\varepsilon/L_1)][1 - e^{-(\lambda+\rho\varepsilon/L_1)t}] \\
&+ [A_2\, e^{-\rho z/L_2}/(\lambda + \rho\varepsilon/L_2)][1 - e^{-(\lambda+\rho\varepsilon/L_2)t}] \\
&+ [B\, e^{-\rho z/L_3}/(\lambda + \rho\varepsilon/L_3)][1 - e^{-(\lambda+\rho\varepsilon/L_3)t}]
\end{aligned} \tag{2}
$$

where A_1 and A_2 are constants related to production by slow muons (0.096 and 0.021 for Be and 0.723 and 0.156 for Al respectively), B is a constant related to production by fast muons (0.026 and 0.192 for Be and Al respectively), and L_1, L_2, and L_3 are cosmic ray mean free paths (738.6 g cm^{-2}, 2688 g cm^{-2}, 4360 g cm^{-2}).

Glacial erosion is a non-steady-state process in glacial valley evolution. During glacial overriding, TCN production stops because the ice shields rock from cosmic radiation and the existing TCN concentration decreases in direct proportion to the amount of rock removed by glacial erosion. TCN loss by radioactive decay during the glacial event is insignificant unless the ice shields the rock continuously for more than 100 ka (Fabel and Harbor 1999). In some cases, bedrock erosion by ice may not be sufficient to completely remove the existing TCN inventory, leaving behind glacially abraded surfaces with TCN inheritance (Figure 1A). This potentially introduces significant errors in surface exposure dating (Fabel et al. 1997; Colgan et al. 2002). However, in some circumstances, TCN inheritance can be constrained and used to estimate the amount of material removed during a glacial erosion event (Briner and Swanson 1998; Davis et al. 1999; Colgan et al. 2002).

To use TCNs as glacial erosion monitors requires determination of the TCN inventory accumulated prior to and since the last deglaciation. For a glacially eroded site TCN inheritance (N_{inh}) in a sample is given by:

$$
N_{inh} = N_{meas} - N_{deg} \tag{3}
$$

where N_{meas} is the measured TCN concentration and N_{deg} is the concentration accumulated since the last deglaciation. For samples where $N_{inh} \leq 0$ the entire TCN inventory accumulated prior to the last glacial event has been removed, while $N_{inh} > 0$ indicates incomplete glacial scouring. Zero glacial erosion is indicated when N_{inh} equals the modeled TCN inventory accumulated during the interglacial period before the last glacial event (N_{inter}). Comparing N_{inh} between different samples collected along a valley cross section yields a first order approximation of the variability of glacial erosion along that section even if the deglaciation
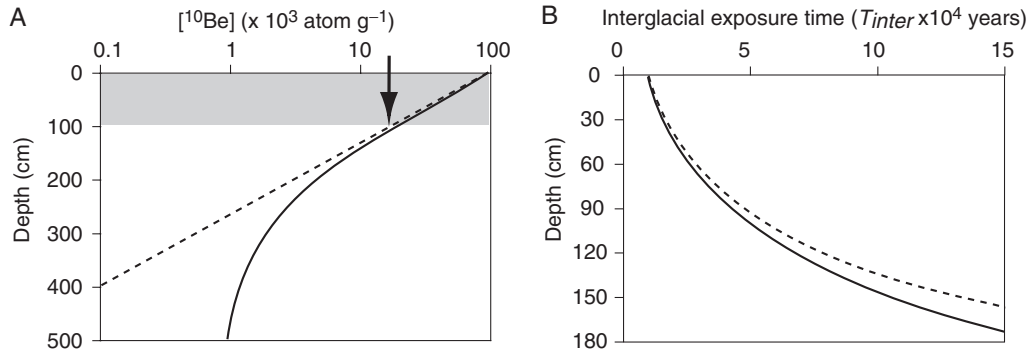

Figure 1. (A) ^{10}Be concentration vs. depth after 20ka exposure calculated using equation 1 for nucleon production (dashed line) and equation 2 for combined nucleon and muon production (solid curve) with a surface production rate of 5.1 atoms g^{-1} a^{-1}, a rock density of 2.75 g cm^{-3} and no erosion. Note the divergence of the curves and the resulting difference in depth estimates if muon production is neglected. If this rock undergoes a rapid erosive event that removes 100 cm of rock (shaded area) after being exposed for 20ka then the new rock surface contains an inherited TCN concentration (arrow) from the previous exposure. (B) Variation in calculated depth for a ^{10}Be inheritance of 50000 atoms g^{-1} as a result of increasing the interglacial exposure time (T_{inter}) calculated for nucleon (dashed curve) and for combined nucleon and muon production (solid curve) using the same production rate, density, and erosion rate as in (A).

and interglacial times are not well constrained. However, to estimate the depth of rock removed using N_{inh} requires determination of N_{deg} and N_{inter} because the depth at which the TCN concentration in a sample equals N_{inh} depends on the exposure duration prior to the erosive event (Figure 1B). The time since the last deglaciation (T_{deg}) and the duration of the previous interglacial (T_{inter}) are needed to calculate N_{deg} and N_{inter} using equations 1 or 2. In this study the penultimate and last deglaciation ages are determined from TCN surface exposure ages. The difference between these ages is used as the interglacial time (T_{inter}). The depth (z) of rock removed can be calculated for the nucleons only case

(equation 1) according to:

$$z = -\ln(N_{inter}/N_{inh})\,\Lambda/\rho \qquad (4)$$

or, to include production by muons, it can be calculated numerically using equation 2 with $t = T_{inter}$. Uncertainties in T_{inter} arising from uncertainties in the estimates of the last and penultimate deglaciation ages, and surface erosion and/or shielding during interglacial times, can lead to significant variation in the depth estimates (Figure 2). If T_{inter} is underestimated the calculated depth removed will be an overestimate and vice versa (Figure 2). Many of the uncertainties cannot be easily constrained; therefore, we start with these initial
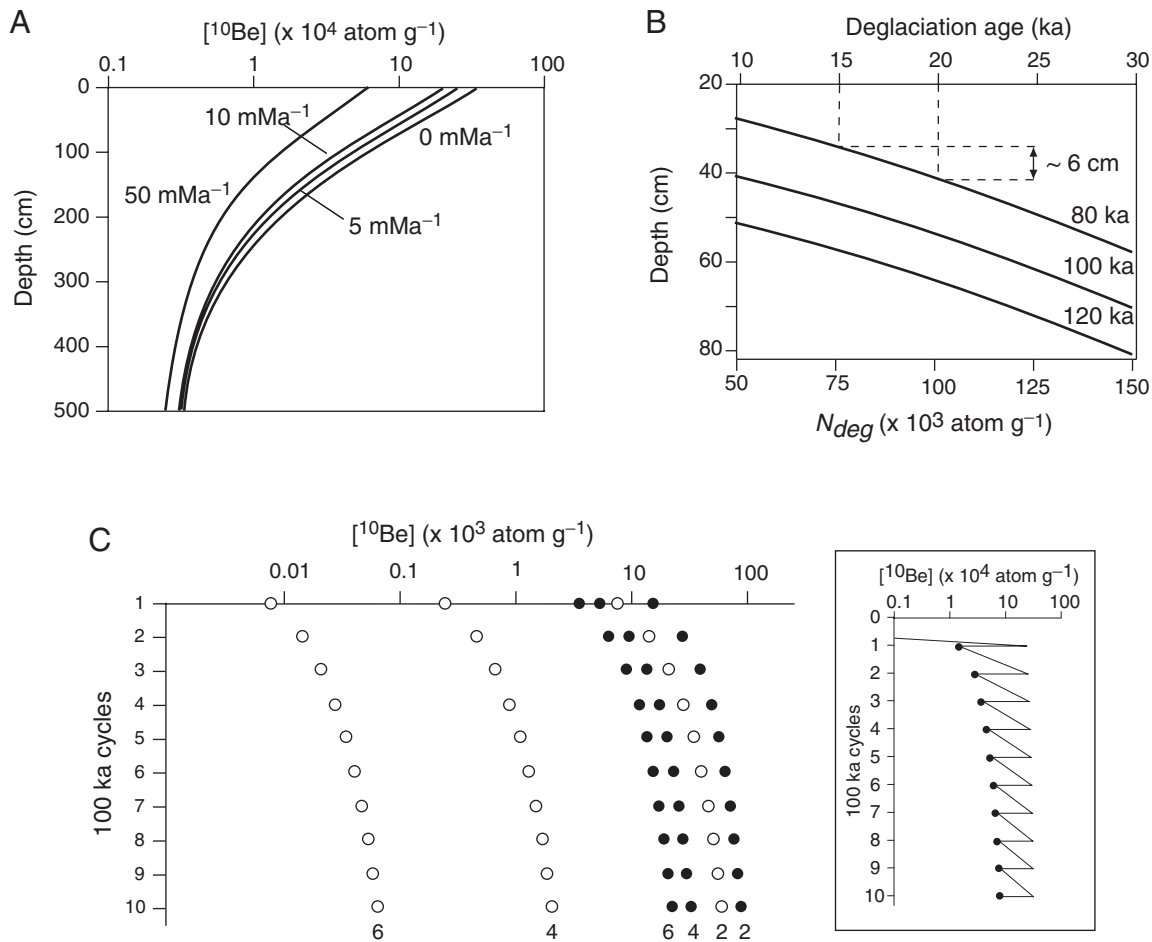

Figure 2. Curves showing the effects of varying interglacial erosion, interglacial exposure time and deglaciation ages on [10]Be depth profiles and glacial erosion depth estimates. All curves are calculated for nucleons only with a [10]Be surface production rate of 5.1 atoms g^{-1} a^{-1} and a rock density of 2.75 g cm^{-3}. (A) [10]Be concentration vs. depth after 70ka exposure at different erosion rates (labeled). (B) Variation in estimated depth of rock removed calculated for different deglaciation ages and interglacial exposure times (labelled curves) calculated using zero erosion and $N_{meas} = 3 \times 10^5$ atoms g^{-1}. Under or overestimating the deglaciation age by 5 ka would introduce a ~ 6 cm error in the estimated depth of glacial erosion. (C) Modelled [10]Be inheritance in a rock surface that has undergone a history of rapid glacial erosion every 100ka. The history is repeated for 10 cycles (see inset) and [10]Be inheritance is calculated with 2, 4, and 6m of erosion (labelled curves) after every cycle for nucleon production (open circles) and combined nucleon and muon production (dots). Note that with the inclusion of muon production [10]Be inheritance is substantial even when 6m is eroded every 100ka. In all cases, [10]Be inheritance increases over the modelled 1 Ma history suggesting TCN concentrations measured in any surface suspected to have undergone this style of glacial history should be treated with caution because it is likely a combination of exposure and inheritance.

assumptions: (1) zero interglacial erosion, (2) the sampled surfaces have no TCN inheritance after the penultimate glaciation, and (3) the length of time the sampled surfaces were covered by ice during the final glaciation is zero. Violation of any of these assumptions decreases the value of $T_{inter;}$ hence our calculated depths of rock removed from the bedrock surfaces represent maximum estimates.

Experimental Design, Field Areas and Methods

Harbor (1992) simulated development of a U-shaped valley by coupling a finite-element model of ice flow to
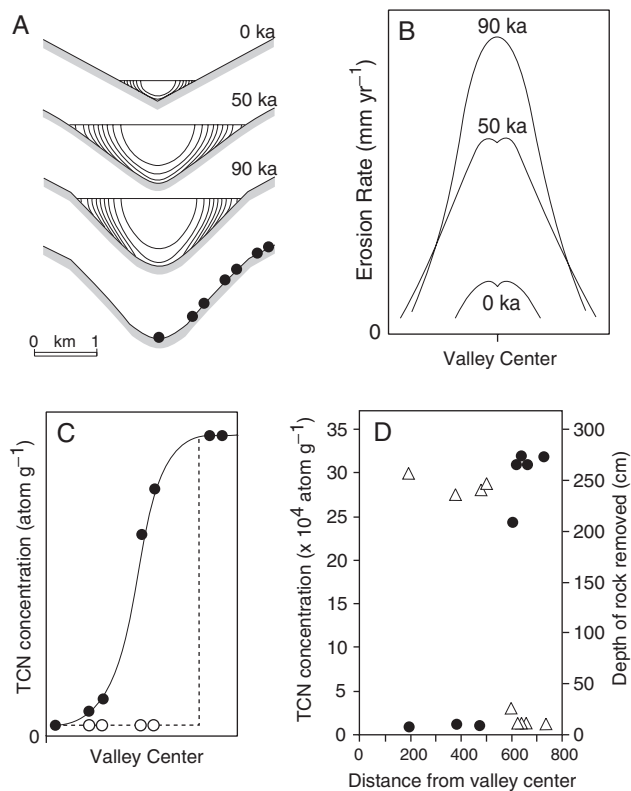

Figure 3. (A) Simulation of cross-section form development over an idealized 100 ka glacial cycle with temporally variable ice discharge. Velocity contours for the glacier sections are in units of 10 percent of the maximum velocity for the section with the central contour in each case at 90 percent (after Harbor 1992). Dots mark hypothetical sample locations shown in (C). (B) Predicted erosion rate plotted for different times during the simulation indicate that erosion decreases toward the lateral limit of the glacier. (C) Hypothetical TCN concentrations in samples collected along a valley transect (A) for the case where deep glacial erosion has completely removed the TCN inventory (open circles) and the case of TCN inheritance due to insufficient glacial erosion (dots). (D) TCN inheritance values (dots) and calculated depths of glacial erosion (triangles) for data reported here from Sinks Canyon, Wyoming (see text and Table 1 for details).

a numerical erosion model and predicted that glacial erosion decreases with increasing distance from the valley center (Figure 3). TCN concentrations in samples collected from the valley center up the valley wall to the limits of glaciation should reflect this decrease, provided the minimum glacial erosion predicted at the top of the glacially eroded section did not completely remove the existing TCN inventory (Figure 3C).

To test the hypothesis that variations in TCN concentrations in samples taken across a glaciated valley can be used to quantify the pattern of bedrock loss due to erosion during the last glaciation, we selected study sites that had been affected by two documented glaciations, with the earlier more extensive than the most recent. Multiple cross sections were used to test for repeatability and to examine whether there is down-glacier variability in the observed erosion pattern. The field areas are located in Sinks Canyon, Wind River Range, Wyoming (Figure 4 and 5) and the South Yuba and Bear River drainages, Sierra Nevada, California (Figure 6).

Sinks Canyon, Wind River Range, Wyoming

The Pleistocene glacial succession is well established for the Wind River Range (Blackwelder 1915; Richmond 1962; Richmond and Murphy 1965; Richmond 1976, 1986). Systematic mapping of the Quaternary stratigraphy of Sinks Canyon (Figures 4 and 5) using relative age characteristics (Dahms 1999) shows that it contains a record of at least three Pleistocene glaciations. Glacial units mapped here include moraines of pre-Bull Lake (O-isotope Stage 12+), Bull Lake (Stage 6), and Pinedale (Stage 2) ages (Pierce, Obradovich, and Friedman 1976; Gosse et al. 1995; Chadwick, Hall, and Phillips

Figure 4. View of Sinks Canyon, Wyoming, looking southwest from the location marked by **X** on the map shown in Figure 5. The arrow points to the top of Profile B.

1997; Hall and Jaworowski 1999). Bull Lake deposits are mapped just above and down-valley of the Pinedale moraines. The Pinedale and Bull Lake moraines partially cover glacially abraded outcrops of Precambrian granite and Cambrian Flathead sandstone.

Samples were collected along two transects located within the mapped limits of the Bull Lake and Pinedale moraines (Figure 5). The highest elevation bedrock sample (97-108) was taken from a position on the north valley wall above mapped glacial units, while all other bedrock samples were taken entirely within the mapped limits of Pinedale moraine units.

South Yuba and Bear Valleys, Sierra Nevada, California

The glacial stratigraphy of the Sierra Nevada is well established (Matthes 1930; Blackwelder 1931; Birkeland 1964; Fullerton 1986; Phillips et al. 1990; Phillips et al. 1996; James et al. 2002). Several well- to moderately-well-preserved middle-to-late Pleistocene glacial stages have been identified in the Sierra Nevada, including the *Mono Basin*, *Tahoe*, *Tenaya*, and *Tioga* advances (in order of decreasing age). The South Yuba and Bear Rivers drain westward from the northwestern Sierra Nevada to the
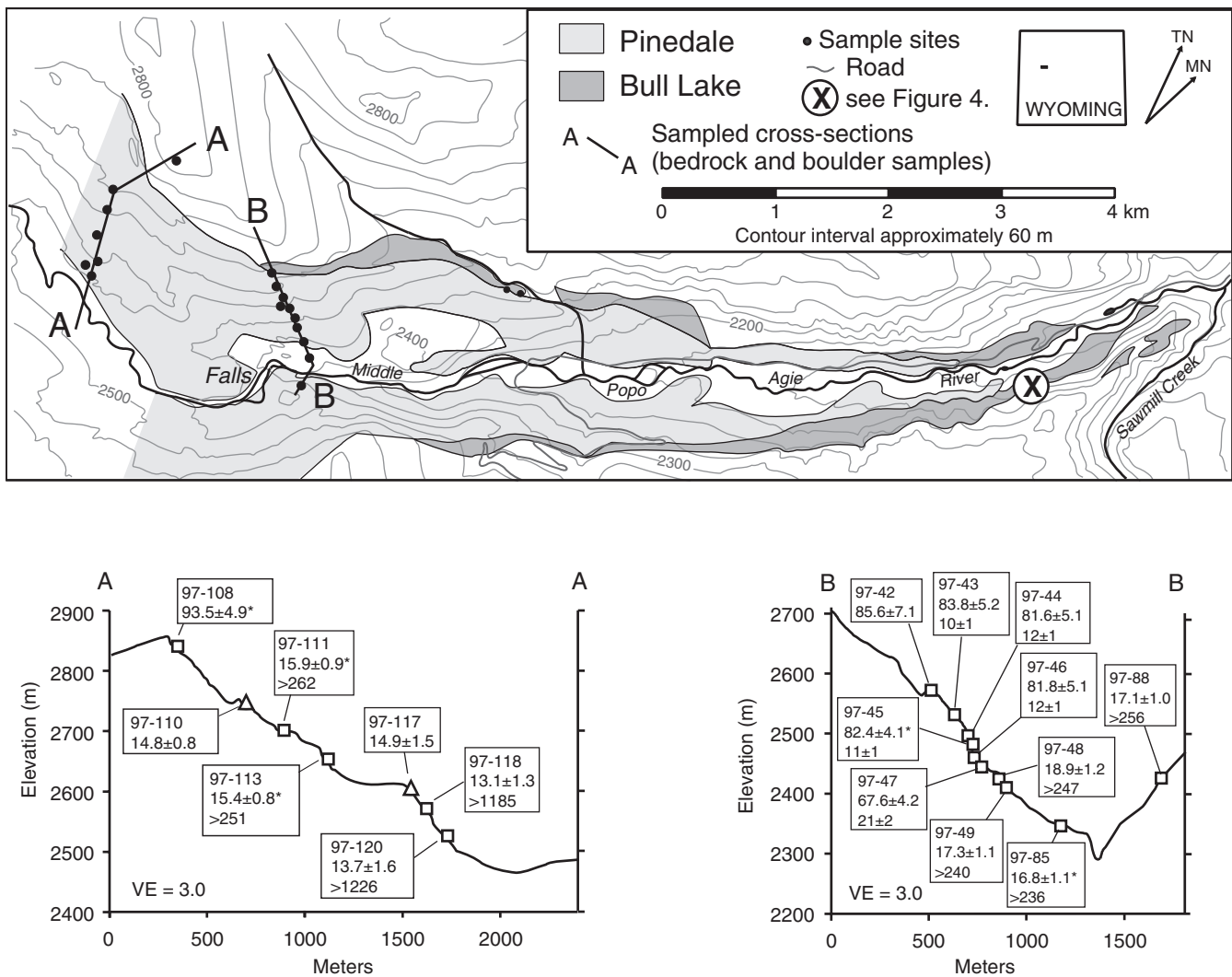

Figure 5. Map of Sinks Canyon showing a simplified distribution of Pinedale and Bull Lake moraines mapped and described by Dahms (1999). Although the shading for the different moraine units is continuous, bedrock outcrops occur along the valley sides (see Figure 4). The cross sections A – A' and B – B' show sample locations, sample numbers, apparent exposure ages, and estimated erosion depths based on nucleon and muon production. Ages marked by an asterisk are average ages from ^{10}Be and ^{26}Al measurements. Triangles and squares on the cross sections indicate samples from erratics and bedrock respectively.
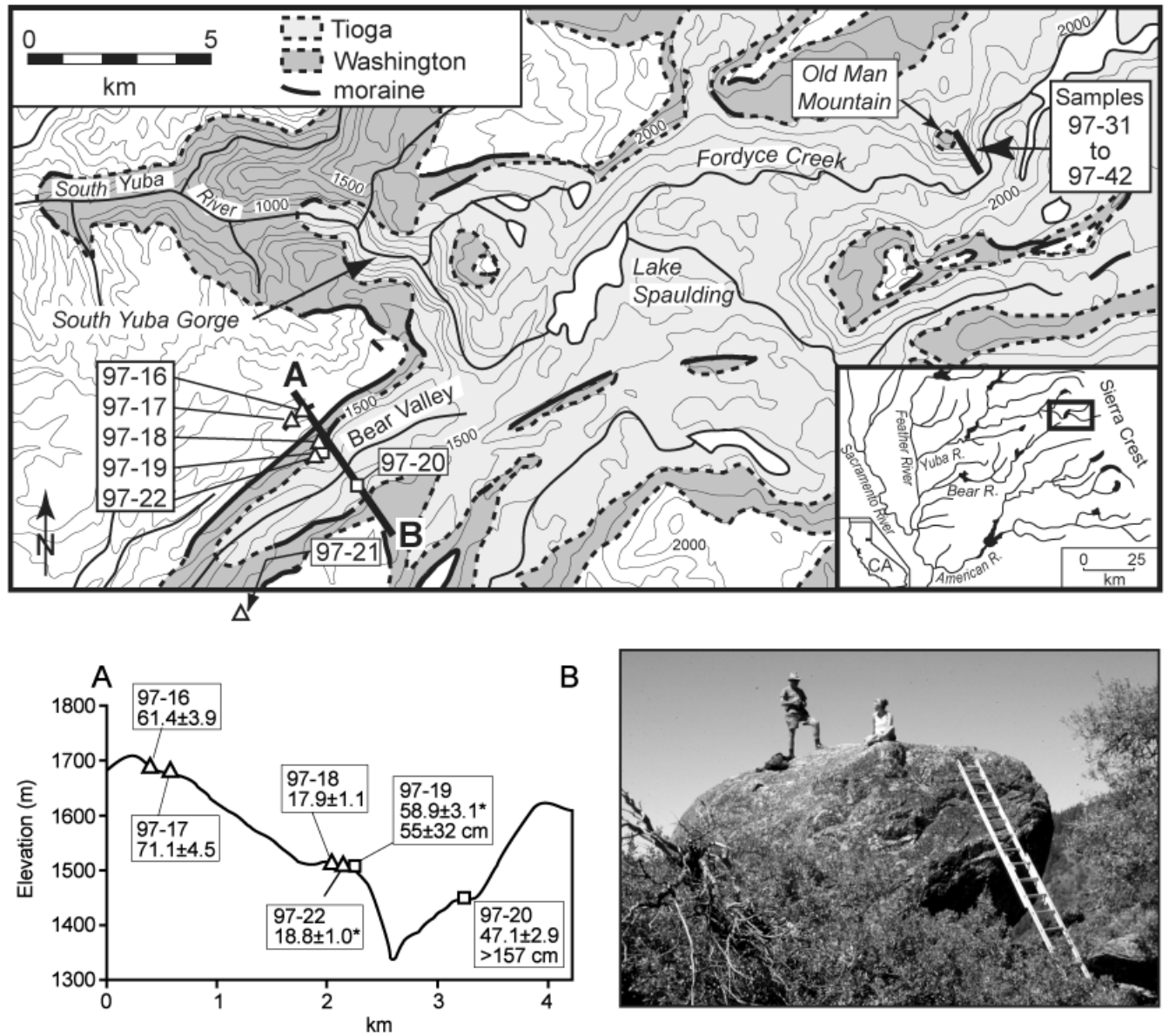
Figure 6. Location of the Sierra Nevada field area (black box in inset). The main map shows the extent of Tioga and Washington ice. Samples were collected from a profile on Old Man Mountain and a profile across Bear Valley (A – B). Triangles and squares indicate samples from erratics and bedrock respectively. Profile A – B shows sample numbers, apparent exposure ages, and estimated erosion depths based on nucleon and muon production across Bear Valley. Ages marked by an asterisk are average ages from ^{10}Be and ^{26}Al measurements. The Old Man Mountain profile is shown in James et al. (2002). Sample 97-22 was collected from the top of the erratic shown in the photo.

Sacramento Valley (Figure 6) and include abundant areas of exposed, glacially striated igneous and metasedimentary rocks. Field mapping documents three glacial stages (James 1995) with the final glaciation being less extensive than previous ones. The glacial chronology for this area was constrained with the same TCN data used here (James et al. 2002). The difference in ages documented by James et al. (2002) and those provided here for the same samples reflects incorporation by this study of changes in direction and intensity of Earth's magnetic field (Ohno

and Hamano 1993; Guyodo and Valet 1999) in the calculation of site-specific production rates (Table 1).

Methods

Bedrock samples were collected from the center of the valley to the penultimate glacial limit. Erratics were sampled to provide additional chronological constraints on the timing of deglaciation. To minimize the impact of

postexposure erosion and shielding, both of which lead to reduction in TCN concentrations, we sampled only striated or polished bedrock surfaces and large erratic boulders located in areas with minimal burial potential. The extent of sample shielding from exposure to cosmic rays by surrounding topography and sample geometry was accounted for in geometric and shielding corrections based on measuring sample surface inclination and vertical angles to the horizon (Dunne, Elmore, and Muzikar 1999). Samples were processed following procedures modified from Kohl and Nishiizumi (1992). Total Al in quartz was measured by atomic absorption spectrometry in aliquots of solutions used to prepare targets for isotopic analysis. Ratios of $^{10}Be/^9Be$ and $^{26}Al/^{27}Al$ for samples and process blanks were measured by accelerator mass spectrometry (AMS) at the Purdue Rare Isotope Measurement Laboratory (PRIME Lab).

Ages were calculated using ^{10}Be and ^{26}Al production rates of 5.1 ± 0.3 and 31.1 ± 1.9 atoms g^{-1} (SiO$_2$) yr^{-1} at 1013 mbar pressure (sea level) and high-latitude respectively (Stone 2000). Production rates are scaled to site-specific altitude and latitude using Stone (2000) and

Table 1. Samples, Sites, Exposure Ages, and Erosion Depth Estimates

Sample No. and Type[a]	Latitude[b] (°)	Longitude[b] (°)	Altitude (m)	Thickness correction	Geometric correction	[Al] quartz (µg g^{-1})[c]	[^{10}Be] atom g^{-1} (× 10^5)[d]	[^{26}Al] atom g^{-1} (× 10^5)
Sinks Canyon Profile A (*Tinter* = 76.0 ± 5.0 ka)								
97-108 w	42.733	251.100	2830	0.992	0.999	30.1	43.9 ± 0.52	232 ± 15
97-110 e	42.729	251.096	2720	0.983	0.997	11.7	5.78 ± 0.07	33.3 ± 2.4
97-111 s	42.727	251.096	2680	0.992	0.997	16.1	6.04 ± 0.07	37.1 ± 5.3
97-113 s	42.728	251.097	2650	0.992	0.979	19.8	5.59 ± 0.09	34.2 ± 2.5
97-117 e	42.723	251.097	2590	0.992	0.998	9.2		32.3 ± 2.7
97-118 s	42.723	251.097	2560	0.992	0.985	12.6		27.3 ± 2.1
97-120 p	42.722	251.097	2520	0.992	0.989	9.5		27.8 ± 2.8
Sinks Canyon Profile B (*Tinter* = 78.8 ± 5.1 ka)								
97-42 w	42.726	251.115	2560	0.983	0.998	41.4		193 ± 9.8
97-43 p	42.727	251.116	2530	0.992	0.652		20.1 ± 0.11	
97-44 s	42.726	251.117	2500	0.958	0.937		26.6 ± 0.16	
97-45 p	42.726	251.116	2480	0.992	0.993	21.8	29.4 ± 0.25	174 ± 8.1
97-46 s	42.725	251.117	2460	0.992	0.988		28.4 ± 0.11	
97-47 p	42.725	251.120	2440	0.992	0.990		23.3 ± 0.19	
97-48 s	42.725	251.119	2420	0.975	0.979		5.91 ± 0.08	
97-49 s	42.723	251.129	2410	0.992	0.989		5.47 ± 0.09	
97-85 p	42.723	251.121	2350	0.992	0.985	20	5.10 ± 0.09	29.8 ± 2.3
97-88 p	42.720	251.121	2450	0.983	0.986		5.49 ± 0.06	
Bear Valley (*Tinter* = 24.8 ± 4.9 ka)								
97-16 e	39.312	239.298	1690	0.992	1.000		11.9 ± 0.19	
97-17 e	39.310	239.289	1680	0.983	0.999		13.6 ± 0.17	
97-19 s	39.298	239.291	1510	0.992	1.000	91.2	10.4 ± 0.11	55.8 ± 4.5
97-20 s	39.293	239.301	1450	0.983	0.998		7.64 ± 0.09	
97-21 e	39.271	239.267	1430	0.983	0.998		7.25 ± 0.14	
97-18 e	39.298	239.291	1510	0.992	1.000		2.84 ± 0.06	
97-22 e	39.298	239.711	1550	0.992	0.999	70.9	3.30 ± 0.06	16.6 ± 1.2
Old Man Mountain (*Tinter* = 32.9 ± 2.6 ka)								
97-31 w	39.372	239.491	1820	0.992	0.988		2.87 ± 0.11	
97-32 p	39.364	239.488	1910	0.992	0.915	242.9		13.3 ± 2.6
97-33 s	39.366	239.486	2000	0.992	0.953	159.7		15.9 ± 2.0
97-35 s	39.366	239.484	2120	0.958	0.941	133.2		14.9 ± 1.6
97-36 p	39.367	239.484	2140	0.992	0.962	171.7		19.6 ± 2.3
97-37 s	39.367	239.485	2160	0.983	0.949	158.2		17.3 ± 2.7
97-38 s	39.368	239.483	2190	0.958	0.996	91.1		18.3 ± 1.7
97-39 s	39.370	239.483	2210	0.983	0.995	147.3		21.3 ± 2.9
97-40 s	39.370	239.483	2240	0.992	0.996	120.3		27.3 ± 2.8
97-41 s	39.372	239.481	2290	0.992	0.995	209.4		13.9 ± 2.7
BB-1B s	39.372	239.600	1990	0.983	1.000	72.6	3.16 ± 0.07	18.2 ± 1.3

Table 1. (continued)

¹⁰Be prod'n rate (atom g⁻¹ yr⁻¹)ᵉ	²⁶Al prod'n rate (atom g⁻¹ yr⁻¹)ᵉ	¹⁰Be age (ka)	²⁶Al age (ka)	¹⁰Be estimated depth removed (cm)	²⁶Al estimated depth removed (cm)
46.8 ± 2.8	283.3 ± 17.2	98.3 ± 6.2	85.5 ± 8.0		
38.7 ± 2.3	234.0 ± 14.2	15.1 ± 0.9	14.3 ± 1.4	>262 (>217)	332 ± 629 (231 ± 439)
38.2 ± 2.3	232.7 ± 14.1	15.9 ± 1.0	16.1 ± 2.5	>252 (>212)	543 ± 1233 (265 ± 602)
36.7 ± 2.2	223.2 ± 13.5	15.4 ± 1.0	15.5 ± 1.5		
	218.0 ± 13.2		14.9 ± 1.5		>1185 (>311)
	208.7 ± 12.6		13.1 ± 1.3		>1226 (>314)
	204.8 ± 12.4		13.7 ± 1.6		
	235.2 ± 14.2		85.6 ± 7.1		17 ± 2 (7 ± 1)
25.0 ± 1.5		83.8 ± 5.2		10 ± 1 (10 ± 1)	
34.0 ± 2.0		81.6 ± 5.1		12 ± 1 (12 ± 1)	
36.8 ± 2.2	223.6 ± 13.5	83.3 ± 5.2	81.1 ± 6.4	10 ± 1 (11 ± 1)	11 ± 2 (11 ± 1)
36.1 ± 2.1		81.8 ± 5.1		12 ± 1 (12 ± 1)	
35.6 ± 2.1		67.6 ± 4.2		26 ± 3 (26 ± 3)	
31.6 ± 1.9		18.9 ± 1.2		>247 (>209)	
32.0 ± 1.9		17.3 ± 1.1		>240 (>205)	
30.5 ± 1.8	185.1 ± 11.2	16.8 ± 1.1	16.2 ± 1.6	>236 (>203)	>797 (>287)
32.4 ± 1.9		17.1 ± 1.0		>255 (>214)	
20.0 ± 1.2		61.4 ± 3.9			
19.7 ± 1.2		71.1 ± 4.5			
17.4 ± 1.0	106.4 ± 6.5	61.3 ± 3.8	53.8 ± 5.5	35 ± 9 (34 ± 11)	75 ± 56 (71 ± 55)
16.6 ± 0.98		47.1 ± 2.9		>157 (>145)	
16.3 ± 0.97		45.4 ± 2.9			
16.0 ± 0.95		17.9 ± 1.1			
16.7 ± 0.99	99.8 ± 6.1	20.0 ± 1.3	16.8 ± 1.6		
19.5 ± 1.2		14.8 ± 1.1		>141(>132)	
	115.0 ± 7.0		11.7 ± 2.4		>177 (>157)
	128.4 ± 7.8		12.5 ± 1.7		>214 (>181)
	132.1 ± 8.0		11.3 ± 1.4		>231 (>192)
	143.9 ± 8.7		13.7 ± 1.8		>206 (>177)
	141.4 ± 8.6		12.3 ± 2.1		>215 (>182)
	147.9 ± 9.0		12.4 ± 1.4		>278 (>214)
	155.0 ± 9.4		13.9 ± 2.1		>222 (>186)
	163.1 ± 9.9		16.9 ± 2.0		142 ± 102 (130 ± 94)
	161.7 ± 9.8		8.7 ± 1.8		>189 (>165)
22.1 ± 1.3	133.7 ± 8.1	14.4 ± 0.92	13.7 ± 1.3	>205 (>182)	>315 (>227)

[a] w = weathered bedrock, s = striated bedrock, p = polished bedrock, e = erratic boulder.

[b] Geographic (in decimal degrees).

[c] Total Al concentration in quartz determined by flame atomic absorption spectrometry and assigned 5% uncertainty.

[d] Data are normalized to NIST SRM 4325 assuming ¹⁰Be/⁹Be = 3.05 × 10⁻¹¹. Carrier ¹⁰Be/⁹Be = 1 × 10⁻¹⁵.

[e] Scaled to geomagnetic latitude (see text for details) and assuming no erosion. Altitude/latitude scaling factors based on those of Stone (2000).

to an effective geomagnetic latitude calculated by the method of Nishiizumi et al. (1989), modified to include changes in dipole orientation over the past 10 ka. Prior to 10 ka a centered dipole field is assumed. The corrections are based on palaeomagnetic intensity records of Ohno and Hamano (1993) and Guyodo and Valet (1999), with dipole orientations specified by Ohno and Hamano (1993). Uncertainties in single-nuclide apparent exposure ages are fully propagated assuming un-correlated random errors in each parameter, including AMS analytical uncertainties, 5 percent uncertainty in total [Al] measurements, and 3 percent uncertainty in decay constants. For several samples we measured both ¹⁰Be and ²⁶Al as a check on internal consistency in laboratory analysis and AMS measurement. The mean ages calculated for these samples are the error-weighted means of the ¹⁰Be and ²⁶Al ages. All other mean ages reported here are arithmetic means (Table 1). Ages

derived from moraine boulders are interpreted as indicating the temporal extent of ice limits.

Note that the ages reported in Table 1 do not include uncertainties associated with latitude/altitude scaling factors and are not intended as calendar ages. The ages are only used for comparison between samples and to set temporal limits for glaciations to facilitate calculation of depth of rock removed. Depth of rock removed during the last glaciation is calculated for bedrock surfaces only (Table 1). Errors in the estimated depths are large when the calculated TCN inheritance (N_{inh}) is small because the fractional error in N_{inh} is the square root of the sum of the squares of the fractional errors in N_{meas} and N_{deg}. For samples where N_{inh} is less than the minimum TCN concentration that could have been calculated within the constraints of the procedural blank measurements ($^{10}Be/^{9}Be = 5 \times 10^{-15}$ and $^{26}Al/^{27}Al = 12.5 \times 10^{-15}$) depths were estimated by setting N_{inh} to this minimum TCN concentration (Table 1). These depths are minimum estimates. The depths of rock removed are reported in two ways; the first value represents the result for production by nucleons and muons, and the second (parenthical) value for nucleons only (equation 4).

Results and Interpretation

Sinks Canyon, Wind River Range

Profile A. Profile A (Figure 5) consists of eight samples covering an elevation range of ~ 310 m. The uppermost sample (97-108) was collected from glacially molded, but weathered, bedrock above the mapped Pinedale glacial limits and provides a minimum mean ^{10}Be and ^{26}Al age of 93.5 ± 4.9 ka (Table 1). Although Bull Lake glacial deposits have not been mapped at this location, the age compares well with published ^{10}Be and ^{36}Cl ages for Bull Lake moraine boulders collected at Fremont Lake on the western side, and at Bull Lake on the eastern side of the Wind River Range (Phillips et al. 1997) and lends confidence to our discrimination between glacial units in the field. The bedrock and erratic samples collected within the Pinedale glacial limits have a mean exposure age of 14.6 ± 1.2 ka, which fits well with the chronology for Pinedale deglaciation in this region (Gosse et al. 1995).

Depth of rock removed was calculated using an interglacial period T_{inter} of 78.9 ± 5.0 ka derived from subtracting the Pinedale deglaciation age of 14.6 ± 1.2 ka from the Bull Lake age of 93.5 ± 4.9 (Table 1). The results from within the Pinedale glacial limits range from >314 (1226) cm at the base of the section (97-

120) to 232 ± 439 (332 ± 629) cm for ^{26}Al and >218 (>262) cm for ^{10}Be at the highest bedrock site (Figure 5). Although at 1σ error the values derived using equation 3 overlap these results are interpreted as indicating a decrease in glacial erosion with elevation because the value at the base of the section is a minimum, while the value for ^{26}Al at the top is a maximum given the assumptions used (see above). The parenthesized values clearly demonstrate that neglecting muon production results in underestimating the depths, especially when the inherited TCN concentration is low.

Profile B. Sinks Canyon Profile B is 2km down-valley from Profile A. The top five samples within the limits of Pinedale glaciation (Figure 5) are statistically indistinguishable and provide a mean age of 83.0 ± 5.3 ka, slightly younger than the oldest age along Profile A. These ages suggest that, except for minor surface striation and polishing, the sampled surfaces remained largely intact during Pinedale glaciation. The four samples below 2440 m elevation (Figure 5) have statistically identical apparent ages with a mean of 17.5 ± 1.0 ka. This is within the range of reported ages for Pinedale glaciation (Pierce, Obradovich, and Friedman 1976; Gosse et al. 1995; Chadwick, Hall, and Phillips 1997; Phillips et al. 1997; Hall and Jaworowski 1999), and is 2.8 ± 1.6 ka older than the mean value 2 km up-valley along Profile A. The exposure age transition between deglaciation and older ages occurs over a vertical distance of 40 m with an intermediate age of 67.6 ± 4.2 ka at 2440 m separating the two groups.

The increase in apparent exposure ages ~ 120m above the valley floor, is reflected in the calculated erosion depths. A T_{inter} value of 76.0 ± 5.0 ka, derived from the local deglaciation age and the same penultimate glaciation age as for Profile A yields erosion depths >203 (236) cm for the lowest four samples (Figure 5), including a sample collected on the opposite valley wall (97-88). Above these samples the depth of rock removed decreases rapidly up the profile from 26 ± 4 (26 ± 4) cm to a mean of 10 ± 2 (12 ± 3) cm for the top 5 samples.

Sierra Nevada, California

Bear Valley. The two highest moraine samples give apparent ages of 61.4 ± 3.9 ka (sample 97-16) and 71.1 ± 4.5 ka (sample 97-17). Following the rationale of Phillips et al. (1990) we favor the older age as the minimum age of the glacial event during which ice extended up to at least ~ 360 m above the present

valley floor in this section of the valley (Figure 6). These boulders lie approximately 100 m above the well-defined moraine of the Washington alloformation (James et al. 2002). A single boulder from the equivalent of this moraine on the opposite side of the valley yields an apparent exposure age of 45.4 ± 2.9 ka (sample 97-21). Based on this cosmogenic age and a > 47.5 ^{14}C ka age from a soil on the same moraine, James et al. (2002) argue for the existence of a middle Wisconsinan glaciation in Bear Valley. Two erratic boulders on a striated bedrock bench 100 m below the Washington moraine (Figure 6) yield a mean age of 18.4 ± 1.1 ka (Table 1), indicating much later ice occupation of this section of the valley with lower ice surface levels than those indicated by the older moraines. The apparent ages of the striated bench (97-19), and another striated bedrock bench 60 m lower on the opposite valley side (97-20) are 58.9 ± 3.1 ka and 47.1 ± 2.9 ka respectively (Figure 6).

The two striated bedrock benches were overridden by ice at least three times, with the most recent event depositing the erratics on the upper bench at 18.4 ± 1.1 ka. The apparent exposure age of the lower bench is statistically the same as the age of the boulder on the Washington moraine (97-21), suggesting that sufficient bedrock erosion took place during the Washington glaciation at 46.3 ± 2.1 ka (weighted mean of 97-20 and 97-21) to completely remove any existing TCN inventory from this bench. If this was the case, and the earlier (71.1 ± 4.5 ka) glacial event had completely removed the TCN inventory at both bedrock sites, then 55 ± 32 (53 ± 34) cm and > 157 (> 145) cm was removed from the upper and lower bench respectively. However, this means the final glaciation at 18.4 ± 1.1 ka did not erode any bedrock and the striations simply indicate very minor surface modification. Alternatively, but less likely, is that the Washington glaciation did not erode the bedrock benches. In this case, all the erosion occurred during the final glaciation with the calculated maximum removal of 19 ± 3 (19 ± 3) cm and 38 ± 5 (37 ± 4) cm of bedrock from the upper and lower bench respectively. Regardless of the scenario used, the results indicate a statistically distinguishable difference in erosion with elevation. Because of the similarity in the bedrock (97-20) and erratic (97-21) ages, we favor erosion during the Washington glaciation rather than the less extensive final glaciation.

Old Man Mountain. Over an elevation range of 470 m, from valley floor to 70 m below the summit, the bedrock exposure ages are very consistent (Table 1) and constrain the deglaciation age to a mean of 13.4 ± 1.7 ka (not including 97-41). Sample BB-1B, with an exposure age of 14.2 ± 0.8 ka, was collected from the top of a nearby unnamed butte (James et al. 2002) and confirms the mean deglaciation age derived from Old Man Mountain. These data illustrate the reproducibility of the TCN technique, and show that in heavily scoured landscapes similar deglaciation ages are found, regardless of position on a valley wall. The apparent age of sample 97-41 is considerably lower than for the other samples (Table 1). Unlike the other samples that were collected from exposed slopes, this sample was collected from a striated surface located in a depression. The depression may have retained ice, snow, or till that partially shielded the sample, resulting in a lower TCN concentration. Seasonal shielding by snow alone seems unlikely because the difference in TCN concentration between sample 97-41 and the next lowest sample can only be explained if sample 97-41 was covered by ~ 8 m of snow (density $= 0.3$ g cm^{-3}) for six months of every year since deglaciation. Without analysis of more samples from the same location it is not possible to determine if the much younger exposure age is due to a measurement problem or if it really reflects a more complicated exposure history that currently cannot be resolved.

The relatively uniform exposure ages along the profile indicate that this flank of Old Man Mountain underwent considerable glacial erosion. Using the Bear Valley penultimate glaciation age of 46.3 ± 2.1 ka, the estimated minimum depth of rock removed during the last glaciation is 141 (132) cm at all sites except 97-40 where the calculation yields a maximum of 142 ± 102 (130 ± 94) cm (Table 1).

Discussion

Both in the Sierra Nevada and the Wind River Range, two types of valley cross section were encountered: one in which the entire area within the limit of the last glacial advance has TCN concentrations indicative of extensive scour and one in which differential bedrock loss with elevation occurred. For the pervasively scoured cross sections, it is not possible to determine a pattern of bedrock loss. The consistent exposure ages indicate that in an area that has undergone a major rock removal event, TCN-exposure age dating provides statistically similar ages from sample sites with wide variations in landscape position. It is not necessary, for example, to restrict sampling to surfaces at the valley bottom to get a deglaciation age at Old Man Mountain because even steep surfaces well up the valley wall give the same age as valley bottom sites.

For cross sections with clear evidence of differential bedrock loss, there is a clear pattern of decreasing glacial

erosion with increasing distance from the valley axis, as predicted by numerical models (Harbor 1992 and Figure 4). An important issue is whether the estimated bedrock loss is solely a result of variations in the efficiency of glacial erosion or if other processes are also responsible. The method used to calculate erosion depths from TCN inheritance does not allow differentiation between glacial and nonglacial erosion. Several lines of evidence, however, suggest that glacial erosion is the dominant form of rock loss at the sites. The fact that striations, which are often less than 2 mm deep, have not been removed after as much as ~ 18 ka of exposure suggests that postglacial bedrock loss on glacially scoured surfaces is a slow process. Although weathering has obliterated striations on bedrock outcrops outside the limits of the last glaciation the coincidence of the [10]Be age for sample 97-108 in Sinks Canyon and previously published [10]Be ages for Bull Lake glaciation (Phillips et al. 1997), indicates that very little material has been eroded from this surface. We conclude that subaerial erosion is a minor component in the overall development of our study sites in Sinks Canyon since Bull Lake glaciation. Similarly, the presence of old striated bedrock surfaces in Bear Valley (Sierra Nevada) indicates insignificant interglacial erosion at these sites. Obviously, our sampling was biased toward striated surfaces, and our conclusions are therefore not necessarily valid for those areas that are not striated. However, the key point is that if interglacial erosion had been a significant factor at any of our sites, the calculated depths of rock removed by glacial erosion would decrease, but the pattern of glacial erosion would remain the same (Figure 2).

The assumption that the penultimate glaciation eroded enough rock to remove the inherited TCN depth profile from sampled sections is more difficult to sustain. The last glaciation obviously did not remove enough rock at some sites, so why should the penultimate glaciation? At the selected localities the penultimate glaciation was more extensive than the final glaciation as shown by field mapping. Thus the sampled profiles would have been covered by more ice, albeit not much more, which would have led to greater erosion, as suggested by numerical models (Harbor 1992) and the data reported here. The long-term erosion history of our sites could also contribute significant TCN inheritance (Figure 2C), but, as with complete TCN removal, it is not possible to verify this. If the penultimate glaciation had left behind surfaces with existing TCN concentrations, then our estimates of rock loss due to the last glaciation are maximum values.

Each field site has particular characteristics that might explain some of the differences in erosion between the upstream and downstream sections. Bear Valley is a very low gradient, perched valley on a branching glacier (James et al. 2002). Ice flowed over a high ledge to get into Bear Valley, with most of the ice flow going down the steeper and deeper South Yuba gorge. The bedrock benches that were sampled are near the Tioga terminus and constrict the valley (Figure 6). While the constriction could result in higher erosion rates if ice velocities were high, in this terminal zone of a low-gradient branching glacier, flow velocities were probably low. Further upstream, at Old Man Mountain, ice was flowing in a narrow, steep canyon and was forced to turn sharply by the western flank of the mountain (Figure 6). We would expect more efficient glacial erosion there than in Bear Valley.

In Sinks Canyon there is a prominent bedrock step (Middle Popo Agie Falls) and moraine between Profiles A and B. Above this step, glacial erosion has scoured the valley, removing the inherited cosmogenic nuclides (Profile A). Below the step we find TCN inheritance 120 m above the valley floor (Profile B). The profiles are ~ 2 km apart, and Profile A was deglaciated 2.8 ± 1.6 ka later than Profile B. From the TCN perspective, it is interesting to note that over such a short distance, we cross a threshold from complete removal of the preglacial TCN inventory to a distinct pattern of inheritance. One reason for this could be that ice velocities are typically lower below a bedrock step, and, therefore, we would expect velocity-driven erosion processes to be reduced here.

The results reported here suggest great variability in glacial erosion rates between sites in the same glacial valleys. Such variability in erosion rates is in part explained by ice velocity changes along and across glaciers, and in part by local controls that produce significant variations superimposed on more general trends. Given these complexities, the three-dimensional aspects of ice flow need to be considered in glacial erosion studies, not simply the position within a valley cross section.

Conclusions

Terrestrial cosmogenic nuclide (TCN) measurements demonstrate that along valley-side transects in the Wind River Range, Wyoming, and the Sierra Nevada, California, apparent surface exposure ages and TCN inheritance can be used to provide important constraints on spatial and temporal patterns of glacial occupation and erosion on a valley scale. Both valleys experienced at least two glacial advances that produced erosion. In each case, valley transects recorded erosion that decreased

toward the lateral limit of ice extent, while further upstream, valley transects recorded pervasive erosion throughout. The amount of bedrock removed during a glaciation was calculated from TCN inheritance in glacially striated surfaces. Failure to incorporate TCN production by muons leads to significant underestimates of the depth of rock removed.

The results are consistent with previous model predictions for general cross-sectional variations in erosion patterns under temperate valley glaciers (e.g., Harbor 1992). This suggests that more extensive sampling in areas with limited erosional loss may provide detailed records of erosion patterns with which to test models of ice dynamics and erosion processes that use site-specific boundary conditions. Such tests of predicted erosion patterns are critical for improving our understanding of erosion processes and for generating refined predictive equations.

The chronologic implications of the exposure age data for the Sierra Nevada field area are discussed in detail by James et al.(2002). In Sinks Canyon, Wyoming, apparent exposure ages identify two major glacial events in the valley. The first and oldest, dated locally at (93.5 ± 4.9 ka), is correlated to the Bull Lake glaciation. The mean exposure age for the last deglaciation ranges from 14.6 ± 1.2 ka for one profile to 17.5 ± 1.0 ka for a second profile 2 km downstream of the first, and are consistent with data reported for the Pinedale glaciation from other sites in the Wind River Range.

The results presented here contain several implications for the TCN technique. The strong agreement of apparent exposure ages, both within and between sections, and with other studies in nearby areas, confirms the reproducibility of surface exposure dating. TCN inheritance found in striated bedrock near the lateral limits of ice extent indicates that the presence of striations does not necessarily imply deep glacial scouring. TCN inheritance provides a unique opportunity to determine patters of glacial erosion and, under certain conditions, allows the depth of rock removed by glacial erosion to be quantified.

Acknowledgments

References

Bierman, P. R., K. A. Marsella, C. Patterson, P. T. Davis, and M. Caffee. 1999. Mid-Pleistocene cosmogenic minimum-age limits for pre-Wisconsinan glacial surfaces in southwestern Minnesota and southern Baffin Island: A multiple nuclide approach. *Geomorphology* 27 (1–2): 25–39.

Birkeland, P. W. 1964. Pleistocene glaciation of the northern Sierra Nevada, north of Lake Tahoe, California. *Journal of Geology* 2:810–25.

Blackwelder, E. 1915. Cenozoic history of the mountains of central Wyoming. *Journal of Geology* 23:97–117, 193–217, 307–40.

———. 1931. Pleistocene glaciation in the Sierra Nevada and the Basin Ranges. *Geological Society of America Bulletin* 42:865–922.

Boulton, G. S. 1974. Processes and patterns of glacial erosion. In *Glacial Geomorphology*, ed. D. R. Coates, 41–87. London: Allen & Unwin.

Braun, J., D. Zwartz, and J. H. Tomkin. 1999. A new surface-processes model combining glacial and fluvial erosion. *Annals of Glaciology* 28:282–90.

Briner, J. P., and T. W. Swanson. 1998. Using inherited cosmogenic ^{36}Cl to constrain glacial erosion rates of the Cordilleran ice sheet. *Geology* 26 (1): 3–6.

Brown, R. W. 1991. Backstacking apatite fission-track "stratigraphy": A method for resolving the erosional and isostatic rebound components of tectonic uplift histories. *Geology* 19 (1): 74–77.

Bull, W. B. 1991. *Geomorphic response to climate change*. New York: Oxford University Press.

Cerling, T. E., and H. Craig. 1994. Geomorphology and in situ cosmogenic isotopes. *Annual Review of Earth and Planetary Sciences* 22:273–317.

Chadwick, O. A., R. D. Hall, and F. M. Phillips. 1997. Chronology of Pleistocene glacial advances in the central Rocky Mountains. *Geological Society of America Bulletin* 109 (11): 1443–52.

Chorley, R. J., S. A. Schumm, and D. E. Sugden. 1984. *Geomorphology*. London: Methuen & Co., Ltd.

Cockburn, H. A. P., M. A. Seidl, and M. A. Summerfield. 1999. Quantifying denudation rates on inselbergs in the central Namib Desert using in situ-produced cosmogenic ^{10}Be and ^{26}Al. *Geology* 27 (5): 399–402.

Colgan, P. M., P. R. Bierman, D. M. Mickelson, and M. Caffee. 2002. Variation in glacial erosion near the southern margin of the Laurentide Ice Sheet, south-central Wisconsin, USA: Implications for cosmogenic dating of glacial terrains. *Geological Society of America Bulletin* 114 (12): 1581–91.

Dahms, D. E. 1999. Glacial Stratigraphy of Sinks Canyon, Wind River Range, Wyoming. *Geological Society of America Abstracts with Programs* 31 (7): A–57.

Davis, P. T., P. R. Bierman, K. A. Marsella, M. W. Caffee, and J. R. Southon. 1999. Cosmogenic analysis of glacial terrains in the eastern Canadian Arctic: A test for inherited nuclides and the effectivenes of glacial erosion. *Annals of Glaciology* 28:181–88.

Dunne, J., D. Elmore, and P. Muzikar. 1999. Scaling factors for the rates of production of cosmogenic nuclides for geometric shielding and attenuation at depth on sloped surfaces. *Geomorphology* 27 (1–2): 3–11.

Elmore, D., P. Sharma, A. Dunne, S. Vogt, and L. Dep. 1995. The ^{36}Cl-^{36}Cl method for determining both rock erosion rates and exposure times. *EOS* 76:F685.

Fabel, D., and B. L. Finlayson. 1992. Constraining variability in southeast Australia long-term denudation rates using a combined geomorphological and thermochronological approach. *Zeitschrift für Geomorphologie* 36:293–305.

Fabel, D., and J. Harbor. 1999. The use of in-situ produced cosmogenic radionuclides in glaciology and glacial geomorphology. *Annals of Glaciology* 29:103–10.

Fabel, D., J. Stone, L. K. Fifield, and R. G. Cresswell. 1997. Deglaciation of the Vestfold Hills, East Antarctica: Preliminary evidence from exposure dating of three subglacial erratics. In *The Antarctic region: Geological evolution and processes*, ed. C. A. Ricci, 829–34. Siena: Terra Antarctica.

Fabel, D., A. P. Stroeven, J. Harbor, J. Kleman, D. Elmore, and D. Fink. 2002. Landscape preservation under Fennoscandian ice sheets determined from in situ produced ^{10}Be and ^{26}Al. *Earth and Planetary Science Letters* 201:397–406.

Fullerton, D. S. 1986. Chronology and correlation of glacial deposits in the Sierra Nevada, California. *Quaternary Science Reviews* 5:161–69.

Gosse, J. C., J. Klein, E. B. Evenson, B. Lawn, and R. Middleton. 1995. Be-10 Dating of the duration and retreat of the last Pinedale Glacial Sequence. *Science* 268 (5215): 1329–33.

Granger, D. E., and A. L. Smith. 2000. Dating buried sediments using radioactive decay and muogenic production of ^{26}Al and ^{10}Be. *Nuclear Instruments and Methods in Physics Research B* 172 (1–4): 822–26.

Guyodo, Y., and J. -P. Valet. 1999. Global changes in intensity of the Earth's magnetic field during the past 800 kyr. *Nature* 399 (6733): 249–52.

Hall, R. D., and C. Jaworowski. 1999. Reinterpretation of the Cedar Ridge section, Wind River Range, Wyoming: Implications for the glacial chronology of the Rocky Mountains. *Geological Society of America Bulletin* 111: 1233–49.

Harbor, J. M. 1992. Numerical modeling of the development of U-shaped valleys by glacial erosion. *Geological Society of America Bulletin* 104:1364–75.

———. 1995. Development of glacial-valley cross sections under conditions of spatially variable resistance to erosion. *Geomorphology* 14:99–107.

Hofmann, H. J., J. Beer, G. Bonani, H. R. von Gunten, S. Raman, M. Suter, R. L. Walker, W. Wölfli, and D. Zimmerman. 1987. ^{10}Be: Half-life and AMS-standards. *Nuclear Instruments and Methods in Physics Research* B29:32–36.

Howard, A. D., W. E. Dietrich, and M. A. Seidl. 1994. Modeling fluvial erosion on regional continental scales. *Journal of Geophysical Research* 99 (B7): 13971–86.

James, L. A. 1995. Diversion of the upper Bear River: Glacial diffluence and Quaternary erosion, Sierra Nevada, California. *Geomorphology* 14:131–48.

James, L. A., J. Harbor, D. Fabel, D. Dahms, and D. Elmore. 2002. Late Pleistocene glaciations in the northwestern Sierra Nevada, California. *Quaternary Research* 57:409–19.

Johnson, A. M. 1970. *Physical Processes in Geology*. San Francisco: Freeman Cooper and Company.

Kehew, A., L. Nicks, and W. Straw. 1999. Palimpsest tunnel valleys: Evidence for relative timing of advances in an interlobate area of the Laurentide ice sheet. *Annals of Glaciology* 28:47–52.

Kleman, J. 1992. The palimpsest glacial landscape in northwestern Sweden Late Weichselian deglaciation landforms and traces of older west-centered ice sheets. *Geografiska Annaler* 74A:305–25.

Kohl, C. P., and K. Nishiizumi. 1992. Chemical isolation of quartz for measurement of in situ-produced cosmogenic nuclides. *Geochimica et Cosmochimica Acta* 56:3586–87.

Lal, D. 1991. Cosmic-ray labeling of erosion surfaces: In situ nuclide production rates and erosion models. *Earth and Planetary Science Letters* 104:424–39.

Lal, D., and B. Peters. 1967. Cosmic-ray produced radioactivity on the earth. *Handbook of Physics* 46 (2): 551–12.

Matthes, F. E. 1930. Geologic history of the Yosemite Valley: U.S. Geological Survey Professional Paper.

McGee, W. J. 1894. Glacial cañons. *Journal of Geology* 2:350–64.

Merritts, D. J. 1996. The Mendocino triple junction: Active faults, episodic coastal emergence, and rapid uplift. *Journal of Geophysical Research-Solid Earth* 101 (B3): 6051–70.

Morisawa, M. 1976. Tectonics and geomorphic models. In *Theories of landform development*, ed. W. N. Melhorn and R. C. Flemal, 199–216: Binghamton, NY: Binghamton Symposium Proceedings.

Nishiizumi, K., C. P. Kohl, J. R. Arnold, R. Dorn, J. Klein, D. Fink, R. Middleton, and D. Lal. 1993. Role of in situ cosmogenic nuclides ^{10}Be and ^{26}Al in the study of diverse geomorphic processes. *Earth Surface Processes and Landforms* 18:407–25.

Nishiizumi, K., E. L. Winterer, C. P. Kohl, J. Klein, R. Middleton, D. Lal, and J. R. Arnold. 1989. Cosmic ray production rates of ^{10}Be and ^{26}Al in quartz from glacially polished rocks. *Journal of Geophysical Research* 94 (B12): 17907–15.

Norris, T. L., A. J. Gancarz, D. J. Rokop, and K. W. Thomas. 1983. Half-life of ^{26}Al. *Proceedings of the fourteenth Lunar and Planetary Science Conference, Part I, Journal of Geophysical Research* 88 (Supplement): B331–33.

Oberlander, T. M. 1985. Origin of drainage transverse to structures in orogens. In *Tectonic geomorphology*, eds. M. Morisawa and J. T. Hack, 155–82. Boston: Allen & Unwin.

Ohno, M., and Y. Hamano. 1993. Global analysis of the geomagnetic field: Time variations of the dipole moment and the geomagnetic pole in the Holocene. *Journal of Geomagnetism and Geoelectricity* 45:1455–66.

Parent, M., S. Paradis, and A. Doiron. 1996. Palimpsest glacial dispersal trains and their significance for drift prospecting. *Journal of Geochemical Exploration* 56 (2): 123–40.

Phillips, F. M., M. G. Zreda, L. V. Benson, M. A. Plummer, D. Elmore, and P. Sharma. 1996. Chronology for fluctuations in late Pleistocene Sierra Nevada glaciers and lakes. *Science* 274:749–61.

Phillips, F. M., M. G. Zreda, J. C. Gosse, J. Klein, E. B. Evenson, R. D. Hall, O. A. Chadwick, and P. Sharma. 1997. Cosmogenic ^{36}Cl and ^{10}Be ages of Quaternary glacial and fluvial deposits of the Wind River Range, Wyoming. *Geological Society of America Bulletin* 109 (11): 1453–63.

Phillips, F. M., M. G. Zreda, S. S. Smith, D. Elmore, P. W. Kubik, and P. Sharma. 1990. Cosmogenic chlorine-36 chronology for glacial deposits at Bloody Canyon, eastern Sierra Nevada. *Science* 248:1529–32.

Pierce, K. L., J. D. Obradovich, and I. Friedman. 1976. Obsidian hydration dating and correlation of Bull Lake and Pinedale glaciations near West Yellowstone, Montana. *Geological Society of America Bulletin* 87:703–10.

Richmond, G. M. 1962. Three pre-Bull Lake tills in the Wind River Mountains, Wyoming, 132–36. U.S. Geological Survey Professional Paper.

———. 1976. Pleistocene stratigraphy and chronology in the mountains of western Wyoming. In *Quaternary stratigraphy of North America*, ed. W. C. Mahaney, 353–79. Stroudsburg, PA: Dowden, Hutchinson, and Ross.

———. 1986. Stratigraphy and chronology of glaciations in Yellowstone National Park. *Quaternary Science Reviews* 5:83–98.

Richmond, G. M., and J. F. Murphy. 1965. Geologic Map of the Bull Lake East quadrangle, Fremont County, Wyoming: U.S. Geological Survey Geological Quadrangle Map GQ-431, scale 1:24000.

Schumm, S. A. 1977. *The fluvial system*. New York: John Wiley and Sons, Inc.

Selby, M. 1986. *Earth's changing surface*. Oxford: Oxford University Press.

Stone, J. O. 2000. Air pressure and cosmogenic isotope production. *Journal of Geophysical Research* 105 (B10): 23753–59.

Stroeven, A. P., D. Fabel, J. Harbor, C. Hättestrand, and J. Kleman. 2002. Quantifying the erosional impact of the Fennoscandian ice sheet in the Torneträsk-Narvik corridor, northern Sweden, based on cosmogenic radionuclide data. *Geografiska Annaler* 84 (a)(3–4): 275–87.

Sugden, D. E., and B. S. John. 1976. *Glaciers and landscape: A geomorphological approach*. London: Arnold Publishing Co.

Thorn, C. E. 1982. *Space and time in geomorphology*. London: George Allen and Unwin.

Tucker, G., and R. Slingerland. 1994. Drainage basin response to climate change. *Water Resources Research* 33 (8): 2031–47.

Correspondence: Derek Fabel, Research School of Earth Sciences, Australian National University, Canberra, ACT 0200, Australia, e-mail: derek.fabel@anu.edu.au.